Ensemble Data Assimilation applied to RAINEX observations of Hurricane Katrina (2005)

Ryan D. Torn* & Gregory J. Hakim

University of Washington, Seattle, WA

Submitted to *Monthly Weather Review* May 14, 2008

* *Corresponding author address:* Ryan Torn, Department of Atmospheric Sciences, Box 351640, University of Washington, Seattle, WA 98195-1640.

E-mail: torn@atmos.washington.edu

ABSTRACT

An ensemble Kalman filter (EnKF) based on the Weather Research and Forecasting model is applied to generate ensemble analyses and forecasts of Hurricane Katrina (2005) and the surrounding area every six-hours over the lifetime of the storm on a nested domain. These analyses assimilate conventional *in-situ* observations, reconnaissance dropsondes, including data taken during the Hurricane Rainband and Intensity Exchange Experiment (RAINEX), and best track position estimates. Observation assimilation consistently reduces errors in tropical cyclone position, but not in intensity. Analysis increments for observations near the tropical cyclone are dominated by changes in vortex position, and these increments increase the asymmetric structure of the storm.

Dropsondes that sample the synoptic environment provide minimal benefit to the outer domain; however, dropsondes deployed within the TC lead to significant reductions to the position and intensity errors on the inner domain. Specifically, errors in the ensemble-mean six-hour forecasts of minimum pressure are 70% larger when dropsonde data is not assimilated. Precipitation fields are qualitatively similar to TRMM satellite estimates, although model values are generally higher. Moreover, the "spin up" period and initial imbalance in EnKF-initialized WRF forecasts is less than starting the model from a GFS analysis. Ensemble 48-hour forecasts initialized with EnKF analyses have track and intensity errors that are 50% smaller than GFS forecasts and WRF forecasts initialized from the GFS analysis.

1. Introduction

One method of improving numerical weather prediction (NWP) model forecasts of tropical cyclones (TC) is to produce better initial conditions by combining observations with a model forecast via data assimilation. Most operational data assimilation systems employ quasi-fixed error statistics to spread observation information to model grid points; however, these statistics are often not appropriate for the TC environment. Given this difficulty, several different techniques have emerged where either a "bogused" vortex is inserted into the analysis (e.g., Kurihara et al. 1995), or the TC is repositioned to the best-track location during data assimilation (e.g., Liu et al. 2000). These procedures have been tuned to work well for synoptic-scale TC forecasts, but are not adequate for creating meso and convective-scale analyses and forecasts of the storm, particularly for short lead times. The lack of appropriate initial conditions for storm-scale models may contribute to the lack of improvement in TC intensity forecasts during the past 15 years (Rogers et al. 2006).

The ensemble Kalman filter (EnKF) is an attractive approach for TC state estimation because this technique assimilates observations using flow-dependent error statistics, which capture the strong spatial variability near TCs. These flow-dependent error statistics, which control the weight given to observations relative to a short-term forecast and how observational information affects model variables near the TC, should allow for corrections to the TC structure and position without the need for the special techniques described above. Several studies (e.g., Houtekamer et al. 2005; Whitaker et al. 2007; Szunyogh et al. 2008; Torn and Hakim 2008) have shown that assimilating real observations with an EnKF leads to forecasts that are competitive with operational data assimilation systems that incorpo-

rate significantly more data. Moreover, the EnKF produces an ensemble of equally-likely analyses that are available for TC ensemble forecasting, without the need for perturbing deterministic analyses. The interested reader is directed to Evensen (2003) or Hamill (2006) for reviews of the EnKF.

Here we test an EnKF for TC forecasting by implementing such a system to generate analyses and forecasts over the life of Hurricane Katrina (2005). Observations taken during the Hurricane Rainband and Intensity Exchange Experiment (RAINEX) (Houze et al. 2006) provide an opportunity to test the performance of an EnKF for TC forecasting with an unusually rich set of observations. Ensemble analyses and forecasts are generated on a coarse-resolution outer domain, and on a nested, higher-resolution inner domain.

We begin with an overview of the model setup and data assimilation system in section 2. Results for the coarse outer domain are presented in section 3, and the nested inner domain results are shown in section 4. A summary and concluding discussion is given in section 5.

2. Experiment Setup

Gridded analyses of Hurricane Katrina and surrounding locations are generated every six hours by cycling an EnKF from 00 UTC 22 August 2005 (42 hours prior to designation as a tropical depression) to 00 UTC 30 August 2005 (six hours after landfall). The analysis ensemble is advanced in time using version 2.1.2 of the the Advanced Research version of the Weather Research and Forecasting (WRF) model (Skamarock et al. 2005) on a nested domain. The outer domain has 30 km horizontal grid-spacing and covers the eastern United States and northern Caribbean Sea. The inner domain has 10 km horizontal grid-spacing and

covers the Gulf of Mexico and Florida during 12 UTC 26 August to 00 UTC 29 August. Both domains have 38 vertical levels, and use the following components: WRF 3-class microphysics scheme (Hong et al. 2004), Kain-Fritsch cumulus parameterization scheme (Kain and Fritsch 1990), Mellor-Yamada-Janjic boundary-layer scheme (Janjic 2001) and the Noah land-surface model (Ek et al. 2003).

An ensemble of lateral boundary conditions for the outer domain is obtained using the fixed-covariance perturbation (FCP) technique of Torn et al. (2006). Perturbations on the lateral boundaries are derived from random draws from the WRF-VAR system (Barker et al. 2004), scaled by 1.7 and with temporal autocorrelation coefficient of 0.4; these values are taken from Torn and Hakim (2008). These perturbations on the lateral boundaries of the outer domain are centered on 6 hour forecasts of the National Centers for Environmental Prediction (NCEP) Global Forecasting System (GFS). For each inner domain ensemble member, one-way lateral boundary conditions are prescribed by interpolating the corresponding background forecast from the outer domain onto the boundary points of the inner domain. In addition to cycling the data assimilation system, 48-hour ensemble forecasts on the outer domain are generated every 12 hours from 00 UTC 25 August to 00 UTC 27 August by advancing all 90 members with FCP ensemble boundary conditions; the ensemble mean on the lateral boundaries is set to the GFS forecast initialized at the same time.

Observations are assimilated from Automated Surface Observing System (ASOS) stations, ships, buoys, rawinsondes, Aircraft Communications Addressing and Reporting System (ACARS) and cloud motion vectors (Velden et al. 2005) every six hours, and the National Hurricane Center (NHC) TC best-track position (technically the latitude and longitude of lowest sea-level pressure) every three hours, using a square-root version of the

EnKF (Whitaker and Hamill 2002) for a 90 member ensemble. Previous studies have shown that O(100) ensemble members are needed to accurately resolve error covariances, while additional members provide minimal improvement (e.g., Whitaker et al. 2004; Dirren et al. 2007). TC position observations are assimilated similarly to the method described in Chen and Snyder (2007). The NHC best-track estimate of the TC latitude (longitude) is compared to the latitude (longitude) of the minimum SLP in each ensemble member's forecast, and all model state variables are adjusted by this innovation; the NHC position estimates are assumed to have an error standard deviation of 10 km.

These experiments also assimilate targeted dropsondes deployed within one hour of an analysis time by the National Oceanic and Atmospheric Administration (NOAA) Hurricane Research Division (HRD) (e.g., Aberson 2002) and the RAINEX field campaign. Raw dropsonde data often contains high frequency temporal noise that can be problematic for data assimilation, thus we assimilate post-processed data from HRD (e.g., Franklin et al. 1996). Dropsonde drift is accounted for by assimilating the sonde data at the horizontal GPS position of each vertical level. Whereas dropsondes deployed by the NOAA P3 and Naval Research Lab (NRL) P3 sampled the structure of the TC, the NOAA G-IV took observations of the synoptic environment surrounding the storm. Since the outer domain does not have sufficient horizontal resolution to accurately simulate mesoscale TC structures, we decided to exclude all NOAA P3 and NRL P3 data from the set of observations assimilated on the outer domain.

Small ensembles have a tendency to produce spurious long-distance covariances and to underestimate covariance magnitude, which we address with conventional techniques. The influence of observations is localized on both domains using eqn. 4.10 of Gaspari and Cohn

(1999) where the covariances reduce to zero 2500 km from the observation location; vertical localization is not employed. For the outer domain, the deviations from the ensemble mean are inflated by averaging the prior and posterior covariance with a 0.75 and 0.25 weighting, respectively (Zhang et al. 2004). The weighting factors are determined by performing experiments in which these weights are adjusted until the mean-squared error in ensemble-mean six-hour forecasts (computed with respect to rawinsondes) matches the innovation variance; for an optimal ensemble system, these two values should be equal (Houtekamer et al. 2005). Covariance inflation is not applied to the inner domain because it magnifies asymmetries due to TC position during assimilation; this issue will be discussed further in section 4. Torn and Hakim (2008) describe in more detail how the covariance localization radius and weighting factors are determined for similar EnKF studies.

EnKF experiments with global models are often initialized with random climatological states (e.g., Whitaker et al. 2004; Anderson et al. 2005); this approach is problematic on limited-area domains due to a mismatch between this ensemble and the prescribed lateral boundary conditions based on six-hour forecasts. Here, we follow the approach of Dirren et al. (2007) and initialize the outer domain ensemble on 00 UTC 22 August by adding random, scaled, fixed-covariance perturbations from the WRF-VAR system (Barker et al. 2004) to the GFS 36-hour forecast initialized on 12 UTC 20 August. The scaling factor for the perturbations (1.9) is determined by matching the RMS error in this 36 hour forecast to the standard deviation of the WRF-VAR perturbations. After two days of observation cycling, the six-hour forecast errors with respect to observations come into equilibrium with the ensemble variance, which indicates that the ensemble has little memory of the initial data (shown below). The inner domain is initialized at 12 UTC 26 August by pairing each

inner domain ensemble member to an outer domain ensemble member and interpolating the outer ensemble member onto the inner member's grid.

3. Outer Domain Results

Prior to describing the performance of the WRF EnKF forecasts of TC track and intensity, we present verification statistics for two fields with respect to rawinsonde and ASOS observations within the domain. For six-hour WRF EnKF forecasts, we also calculate the observation innovation standard deviation,[1] which should match the RMS error for a well-calibrated ensemble (Houtekamer et al. 2005).

Figure 1 shows that after a 2 day ensemble spin-up period, the RMS error and spread in six-hour WRF EnKF 300 hPa zonal wind and altimeter setting forecasts come into equilibrium. Other fields show similar results and are thus not presented. Over this period, the error in 300 hPa wind (altimeter) is 3.6 m s^{-1} (1.19 hPa), which is 0.4 m s^{-1} larger (0.5 hPa lower) than the error in six-hour GFS forecasts during the same period. Whereas the ensemble spread is generally higher than the RMS error for altimeter, the ensemble is well-calibrated for the 300 hPa wind. The performance of this filter configuration is similar to the real-time EnKF system described by Torn and Hakim (2008).

Analysis and forecasts are verified on the outer domain using position and intensity estimates from NHC best-track data. Table 1 displays the RMS difference between the NHC

[1]This quantity is defined by the square root of the diagonal elements of $\mathbf{H}\mathbf{P}^b\mathbf{H}^{\mathrm{T}} + \mathbf{R}$, where $\mathbf{H}$ is an operator that maps from model state variables to observations, $\mathbf{P}^b$ is the background error covariance matrix, and $\mathbf{R}$ is the observation error variance matrix

best track position and intensity for the ensemble-mean analysis and background forecast (denoted "control"). These quantities are determined by finding the grid point of lowest sea-level pressure (SLP) for each ensemble member. On average, the RMS error in TC track is lower for the ensemble-mean analysis than for the background forecast, which indicates that observation assimilation systematically reduces position errors. We note that although we assimilate best-track position data, the TC position is not a state variable, thus verifying the analysis against best-track data is used to confirm that the flow-dependent error statistics are correcting the ensemble in the appropriate way. The largest position errors occur on 00 UTC 24 August when Katrina is first designated as a tropical depression; however, as the TC intensifies and the circulation becomes better defined, the analysis position errors are consistently less than the horizontal grid spacing. Although these experiments do not assimilate the best-track estimate of TC minimum SLP or maximum surface wind, the RMS errors in minimum SLP for the ensemble-mean analysis and background forecast are less than 15 hPa (Table 1). Furthermore, the error in maximum wind speed[2] is 13 m s^{-1}, which is roughly equivalent to the error in 36 hour official NHC forecasts of Katrina (Beven et al. 2008). For most analysis times, the minimum SLP (maximum wind) on the outer domain is higher (lower) than best track estimates, especially after Katrina undergoes rapid intensification on 28 August.

Table 1 reveals larger errors in the analyses of TC intensity as compared to the background forecast, which indicates that assimilating observations has an adverse impact on TC intensity. To demonstrate how nearby observations affect the TC, Figure 2a shows the SLP

[2]Maximum wind speed in the model is found by computing the highest 10 m wind speed within 250 km of the TC center

increment due to the 500 hPa wind observation taken by a nearby dropsonde at 00 UTC 27 August 2005. Assimilating this observation leads to an increase (decrease) in SLP to the west (east) of the TC center, achieving a shift in the position of the storm to the east. We find that most observations near the TC have a similar increment dipole, indicating that most of the covariance between the TC and surrounding fields is associated with the TC position. To quantify this point, we compute the increment in the ensemble-mean SLP due to sequentially assimilating each observation within 800 km of the TC center at this analysis time. Empirical orthogonal functions (EOF) of these 1000 analysis increments are computed to determine the leading spatial structures that explain the most analysis-increment variance. The leading EOF of the analysis increments, which explains 32% of the increment variance, exhibits a northeast–southwest oriented dipole centered on the TC similar to the single increment shown in Fig. 2a (Fig. 2c). The second EOF, which explains 23% of the variance, also exhibits a dipole centered on the TC, with a different orientation than the leading EOF. The remaining three statistically significant EOFs, which individually explain less than 9% of the variance, and are generally related to the TC intensity and azimuthal wavenumber-two patterns centered on the TC (not shown). Similar patterns are observed when computing EOFs of analysis increments at other times, although the leading EOFs sometimes reflect a mixture of phase and intensity increments.

Excessive variance in TC position can have an adverse affect on the shape and intensity of the TC. For example, assimilating best-track position every six hours, compared to every three hours, produces more variance in TC position, and asymmetric increments that distort the structure of the vortex (not shown). This result indicates that best-track position observations may have an adverse affect on the analysis when the background TC is more

than a few grid points from the best track position.

The value of cycling the data assimilation system is evaluated by comparing the previous results with a deterministic 8-day WRF forecast on the outer domain, initialized on 00 UTC 22 August using GFS analysis for initial and boundary conditions. The tropical wave that evolves into Katrina fails to intensify into a tropical depression in this simulation (not shown). We conclude that continuous observation assimilation yields analysis corrections that are necessary to capture TC genesis in this case. In a separate experiment, dropsonde observations are withheld (denoted as "No Drop" in Table 1). In this case, TC position and intensity RMS errors in the background forecast are nearly identical to the control simulation, suggesting that other observations near the TC, such as the best-track position data, compensate for the absence of dropsondes. When best-track position observations are withheld ("No Best Track" in Table 1), RMS background TC position, minimum SLP and maximum wind speed errors are 64%, 79% and 36% greater, respectively, than the control experiment.

Compared to GFS and deterministic WRF forecasts, the 48 hour ensemble forecasts initialized from the WRF EnKF analyses provide consistently better forecasts of Katrina's track and intensity. Figure 3 shows RMS TC track and intensity errors for forecasts from the WRF EnKF, the GFS, and a WRF forecast on the outer domain using initial and boundary conditions from GFS analyses (WRF-GFS). By hour 48, the RMS error in the WRF EnKF ensemble-mean forecasts of Katrina's track are 60% and 45% lower than GFS and WRF-GFS forecasts, respectively. WRF EnKF forecasts initialized at 00 UTC and 12 UTC 25 August capture the observed southwesterly motion of Katrina, whereas the GFS and WRF-GFS simulations did not (not shown). Since the ensemble-mean lateral boundary conditions for

the WRF EnKF and WRF-GFS forecasts are identical, differences between these forecasts can be attributed entirely to the initial conditions.

WRF EnKF forecasts also have lower errors in TC intensity as compared to the GFS and WRF-GFS forecasts. For all forecast hours, the error in the ensemble-mean is approximately 12 hPa, compared to approximately 28 hPa for the WRF-GFS forecasts. Unlike WRF EnKF analyses, the TC structure is poorly represented in the WRF-GFS initial conditions and the vortex must "spin up" during the first few hours of the simulation; this issue will be further explored in the next section. We note that the large intensity errors in GFS forecasts partially result from the coarse horizontal resolution of the available model output (1° latitude and longitude).

4. Inner Domain Results

Assimilation on the inner domain also produces analysis ensembles that capture well the track and, to a lesser extent, the intensity of Katrina. The RMS error in the TC position is slightly larger than the horizontal grid spacing (Table 1). In contrast to the minimum SLP estimates on the outer domain, the TC minimum SLP in the inner domain analyses are generally too low, although the errors are slightly larger than the outer domain. The largest errors occur around 06 UTC 28 August, because the TC undergoes rapid intensification 12 hours earlier than best track estimates. For maximum wind speed, the errors are smaller than the outer domain; however, these values are typically smaller than the best-track estimate. Assimilating dropsonde data within the TC is important on this domain; the RMS error in the ensemble-mean background forecast of TC position and minimum SLP are 20%

and 70% larger, respectively, when dropsonde data is not assimilated ("No Drop" case in Table 1).

Even though data assimilation is performed independently on each domain, analysis increments on the inner domain show a similar dipole pattern to that obtained on the outer domain (Fig. 2b). Assimilating the dropsonde wind observation northwest of the TC shifts the storm to the east. The leading two EOFs of the SLP analysis increments on this domain are dipoles centered on the TC and explain 25%, 20% of the variance, respectively (Fig. 2d). Other EOFs explain less than 9% of the variance and are related to intensity and azimuthal wavenumber-two structures, as was the case for the outer domain.

As stated in section 2, covariance inflation is not applied on this domain because it led to asymmetric increments to the TC, which distorted its structure. To demonstrate how data assimilation affects the TC structure, we compute a Fourier azimuthal amplitude spectrum of SLP and 850 hPa zonal wind at a distance of 100 km from the TC center for each ensemble member before and after data assimilation. Fig. 4 displays the Fourier amplitude spectrum averaged over all ensemble members[3] at 18 UTC 27 August. This analysis time occurred during an intensive observing period for the RAINEX project, so that there are many dropsondes available for assimilation within the TC. For both fields, the background forecast amplitude spectrum peaks at azimuthal wavenumber one and drops steeply toward higher wavenumbers. The analysis amplitude spectrum is larger at nearly all wavenumbers, but especially at higher wavenumbers, which suggests that data assimilation renders the storm more asymmetric. These results also suggest that integrating the model

[3]Note that because the TC location differs between ensemble members, the mean Fourier spectrum is not equal to the spectrum of the ensemble mean.

acts to reduce the noise introduced by data assimilation; that is, the storm becomes more axi-symmetric during the six-hour forecast. This introduced asymmetry could result from a number of factors, including sampling error due to using a small ensemble and differences in the location and amplitude of convection in each ensemble member.

Although EnKF data assimilation introduces asymmetric noise to the TC structure, the analysis still retains the important TC structures and provides initial conditions sufficient to produce reasonable short-term forecasts of the storm's mesoscale structures. To demonstrate this point, we present three different 45-minute forecasts of precipitation rate initialized at 21 UTC 26 August and compare these results to an estimate from the Tropical Rainfall Measuring Mission (TRMM) satellite valid at the same time. All three forecasts use the same model physics, but have different initial conditions. The initial condition for the "full field" forecast uses a randomly chosen inner domain analysis ensemble member from 21 UTC 26 August. This same initial condition is used for the "cold start" forecast; however, the initial cloud water and rain water mixing ratio fields are set to zero. Differences between the "full field" and "cold start" forecasts thus result from having analyzed or "hot start" microphysical fields. The final forecast (denoted "GFS field") is initialized from the 3 hour GFS forecast valid 21 UTC 26 August, thus differences between this forecast and the "full field" demonstrate the benefit of initializing WRF TC forecasts with EnKF microphysical analyses.

Figure 5 shows that the horizontal distribution of precipitation for the forecasts initialized from inner domain analyses are broadly similar to the TRMM estimate; however, the precipitation is 2.5 times higher in the eastern eyewall for the two forecasts that use EnKF initial conditions. The higher precipitation rate and associated latent heating in the WRF

simulations may explain the persistent low bias in the model's TC minimum central pressure. Furthermore, the EnKF forecast shows a primary rainband that is narrower and displaced north relative to the TRMM estimate.

It is difficult to distinguish between the "full field" and "cold start" precipitation distributions (Fig. 5a-b). This result seems to indicate that having analyzed microphysical fields has little bearing on short-term precipitation forecasts; the model is able to spin-up the appropriate fields in a short amount of time. In contrast, the precipitation distribution for the "GFS field" forecast, which is initialized from a symmetric vortex, is broader than either the "full field" or "cold start" forecasts (Fig. 5d). This result therefore suggests that high-resolution analyses produced by an EnKF system can lead to more realistic short-term forecasts of microphysical fields.

The previous result suggests that WRF EnKF-initialized forecasts may suffer from fewer "spin up" problems during the first few hours of a forecast as compared to using an analysis from a different model. Another measure of the quality of the initial conditions is given by the amount of imbalance (acoustic and gravity wave activity) in the model. To assess this measure we evaluate the RMS value of the time derivative of the dry-air mass field at each grid point within 600 km of the TC center at two minute intervals for a forecasts initialized from an EnKF analysis and from the GFS analysis. Figure 6 shows that this quantity is initially large for both forecasts and decreases to an equilibrium value over approximately 2–3 hours; however, the EnKF-initialized forecast is always less than or equal to the GFS-initialized forecast and equilibrates at an earlier forecast hour. We note that this result also holds for the outer domain, which indicates that WRF TC forecasts initialized from EnKF analyses are less likely to have spin up problems than initializing from another model's analysis.

Furthermore, this calculation also indicates that although data assimilation introduces high-wavenumber noise into the TC, this noise appears to have relatively little impact on the balanced fields after one hour.

5. Discussion and Conclusions

Ensemble analyses and forecasts of Hurricane Katrina are generated on a nested domain using an ensemble Kalman filter based on the WRF model. Conventional *in-situ* observations, reconnaissance dropsondes, and NHC best track estimate data are assimilated every six-hours for the duration of Katrina's lifetime. These experiments show that the EnKF approach performs well for TC data assimilation without employing special schemes such as vortex bogusing and repositioning.

Comparisons with NHC best-track estimates indicate that the EnKF analysis and forecast ensembles on both domains provide accurate estimates of the TC position, and to a lesser extent the TC intensity. On the outer domain, NHC best-track data has a large impact on the TC position, but has little affect on the intensity. Dropsondes that sample the synoptic environment provide minimal benefit to the outer domain; however, dropsondes deployed within the TC lead to significant reductions to the position and intensity errors on the inner domain. Horizontal distributions of precipitation on the inner domain compare qualitatively well with TRMM satellite estimates, except that the model produces a greater amount of precipitation near the center of the storm. This favorable comparison is due to having initial conditions that contain a dynamically consistent three-dimensional representation of the TC, rather than properly analyzed microphysical fields (cf. Figs. 5a, b).

Ensemble forecasts initialized from the WRF EnKF analyses have smaller errors for TC track and intensity compared to GFS forecasts and WRF forecasts on the same domain that are initialized from GFS analyses. Smaller track and intensity errors indicate that the WRF EnKF analyses provide a better estimate of the steering flow and a TC structure that is more compatible with the model, respectively.

WRF forecasts initialized from EnKF analyses have a shorter "spin up" time and contain less initial imbalance as compared to simulations that use initial conditions from the GFS model. As a consequence, high-resolution TC forecasts initialized from an EnKF analysis are less likely to suffer from large convective bursts that may occur during the first six hours (e.g., Davis et al. 2008). If large enough, these convective bursts can significantly alter the TC structure in the short-term, which in turn, can limit the usefulness of longer-term forecasts (Chris Davis, NCAR, Personal Communication).

Analysis increments for a single observation near the TC tend primarily to shift the position of the storm. Excessive variance in the TC position can also produce asymmetric analysis increments, which can erroneously affect the intensity of the storm and introduce noisy asymmetric structures. These asymmetries distort the TC in the analysis, and lead to a weakening of the TC through axi-symmetrization during the first few hours. Assimilating observations before this symmetrization is complete may introduce even more high-wavenumber noise, which would result in short-term intensity forecast errors. This problem of excessive TC position variance can be partially overcome by assimilating TC position at high temporal frequency, thereby decreasing position variance.

Acknowledgments.

We thank Chris Velden and Dave Stettner of CIMSS/SSEC for providing cloud winds for these experiments. This study was made possible in part due to the data made available to the Earth System Research Laboratory/Global Systems Division by the following commercial airlines: American, Delta, Federal Express, Northwest, United, and United Parcel Service. Processed dropsonde data is provided by NOAA Hurricane Research Division of AOML. Stacy Brodzik helped obtain the RAINEX dropsonde data used in this study. This work was supported by NSF Grant ITR-0205648, NOAA CSTAR Grant NA17RJ1232, and ONR Grant N00014-06-1-0510.

REFERENCES

Aberson, S. D., 2002: Two years of operational hurricane synoptic surveillance. *Wea. Forecasting*, **17**, 1101–1110.

Anderson, J. L., B. Wyman, S. Q. Zhang, and T. Hoar, 2005: Assimilation of surface pressure observations using an ensemble filter in an idealized global atmospheric prediction system. *J. Atmos. Sci.*, **62**, 2925–2938.

Barker, D. M., W. Huang, Y. R. Guo, A. J. Bourgeois, and Q. N. Xiao, 2004: A three-dimensional variational data assimilation system for MM5: Implementation and initial results. *Mon. Wea. Rev.*, **132**, 897–914.

Beven, J. L., et al., 2008: Atlantic hurricane season of 2005. *Mon. Wea. Rev.*, **136**, 1109–1173.

Chen, Y. and C. Snyder, 2007: Assimilating vortex position with an ensemble Kalman filter. *Mon. Wea. Rev.*, **135**, 1828–1845.

Davis, C., et al., 2008: Prediction of landfalling hurricanes with the advanced hurricane wrf model. *Mon. Wea. Rev.*, **136**, Accepted.

Dirren, S., R. D. Torn, and G. J. Hakim, 2007: A data assimilation case-study using a limited-area ensemble Kalman filter. *Mon. Wea. Rev.*, **135**, 1455–1473.

Ek, M. B., K. E. Mitchell, Y. Lin, E. Rodgers, P. Grunmann, V. Koren, G. Gayno, and J. D. Tarpley, 2003: Implementation of Noah land surface model advances in the National Centers for Environmental Prediction operational mesoscale Eta model. *J. Geophys. Res.*, **108**, 8851.

Evensen, G., 2003: The ensemble Kalman filter: theoretical formulation and practical implementation. *Ocean Dyn.*, **53**, 343–367.

Franklin, J. L., S. E. Feuer, J. Kaplan, and S. D. Aberson, 1996: Tropical cyclone motion and surrounding flow relationships: Searching for beta-gyres in Omega dropwindsonde datasets. *Mon. Wea. Rev.*, **124**, 64–84.

Gaspari, G. and S. E. Cohn, 1999: Construction of correlation functions in two and three dimensions. *Quart. J. Roy. Met. Soc.*, **125**, 723–757.

Hamill, T. M., 2006: Ensemble-based atmospheric data assimilation: A tutorial. *Predictability of Weather and Climate*, T. Palmer and R. Hagedorn, Eds., Cambridge Press, 124–156.

Hong, S. Y., J. Dudhia, and S. H. Chen, 2004: A revised approach to ice microphysical processes for the bulk parameterization of clouds and precipitation. *Mon. Wea. Rev.*, **132**, 103–120.

Houtekamer, P. L., H. L. Mitchell, G. Pellerin, M. Buehner, M. Charron, L. Spacek, and B. Hansen, 2005: Atmospheric data assimilation with an ensemble Kalman filter: Results with real observations. *Mon. Wea. Rev.*, **133**, 604–620.

Houze, R. A., et al., 2006: The Hurricane Rainband and Intensity Change Experiment:

Observations and modeling of Hurricanes Katrina, Ophelia, and Rita. *Bull. Amer. Meteor. Soc.*, **87**, 1503–1521.

Janjic, Z. I., 2001: Nonsingular implementation of the Mellor-Yamada level 2.5 scheme in the NCEP Meso model. Tech. Rep. NCEP Office Note No. 437, National Centers for Environmental Prediction, 61 pp. pp., Camp Springs, MD.

Kain, J. S. and J. M. Fritsch, 1990: A one-dimensional entraining detraining plume model and its application in convective parameterization. *J. Atmos. Sci.*, **47**, 2784–2802.

Kurihara, Y. M., A. Bender, R. E. Tuleya, and R. J. Ross, 1995: Improvements in the GFDL hurricane prediction system. *Mon. Wea. Rev.*, **123**, 2791–2801.

Liu, Q., T. Marchok, H.-L. Pan, M. Bender, and S. J. Lord, 2000: Improvements in hurricane initialization and forecasting at NCEP with global and regional (GFDL) models. Tech. rep., NOAA Tech. Procedures Bull. 472, 7 pp. pp., Camp Springs, MD.

Rogers, R., et al., 2006: The intensity forecasting experiment. *Bull. Amer. Meteor. Soc.*, **87**, 1523–1537.

Skamarock, W. C., J. B. Klemp, J. Dudhia, D. O. Gill, D. M. Barker, W. Wang, and J. G. Powers, 2005: A description of the Advanced Research WRF Version 2. Tech. Rep. 468+STR, National Center for Atmospheric Research, 88 pp. pp., Boulder, CO.

Szunyogh, I., E. J. Kostelich, G. Gyarmati, E. Kalnay, B. R. Hunt, E. Ott, E. Satterfield, and J. A. Yorke, 2008: A local ensemble transform kalman filter data assimilation system for the ncep global model. *Tellus*, **60**, 113–130.

Torn, R. D. and G. J. Hakim, 2008: Performance characteristics of a pseudo-operational ensemble Kalman filter. *Mon. Wea. Rev.*, **136**, Accpeted.

Torn, R. D., G. J. Hakim, and C. Snyder, 2006: Boundary conditions for limited-area ensemble Kalman filters. *Mon. Wea. Rev.*, **134**, 2490–2502.

Velden, C., et al., 2005: Recent innovations in deriving tropospheric winds from meteorological satellites. *Bull. Amer. Meteor. Soc.*, **86**, 205–223.

Whitaker, J. S., G. P. Compo, X. Wei, and T. M. Hamill, 2004: Reanalysis without radiosondes using ensemble data assimilation. *Mon. Wea. Rev.*, **132**, 1190–1200.

Whitaker, J. S. and T. M. Hamill, 2002: Ensemble data assimilation without perturbed observations. *Mon. Wea. Rev.*, **130**, 1913–1924.

Whitaker, J. S., T. M. Hamill, X. Wei, Y. Song, and Z. Toth, 2007: Ensemble data assimilation with the NCEP Global Forecast System. *Mon. Wea. Rev.*, **135**, Accepted.

Zhang, F., C. Snyder, and J. Sun, 2004: Impacts of initial estimate and observation availability on convective-scale data assimilation with an ensemble Kalman filter. *Mon. Wea. Rev.*, **132**, 1238–1253.

List of Figures

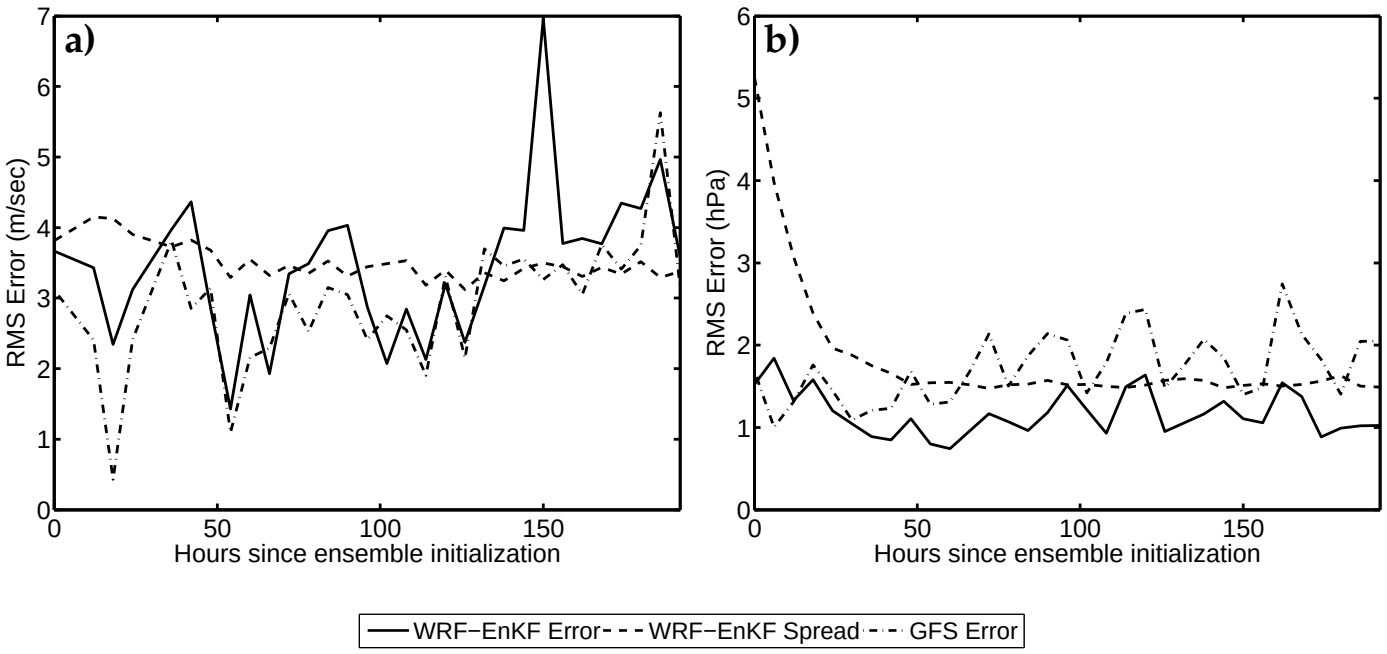

FIG. 1. Time series of the RMS error in WRF EnKF and GFS six-hour forecasts with respect to (a) rawinsonde observations of 300 hPa zonal wind and (b) ASOS observations of altimeter setting in the domain. The dashed line denotes the square root of the sum of the ensemble variance and observation error variance at the observation locations, the solid line the RMS error in the ensemble mean, and the dash-dot line the error in the GFS forecast on this domain.

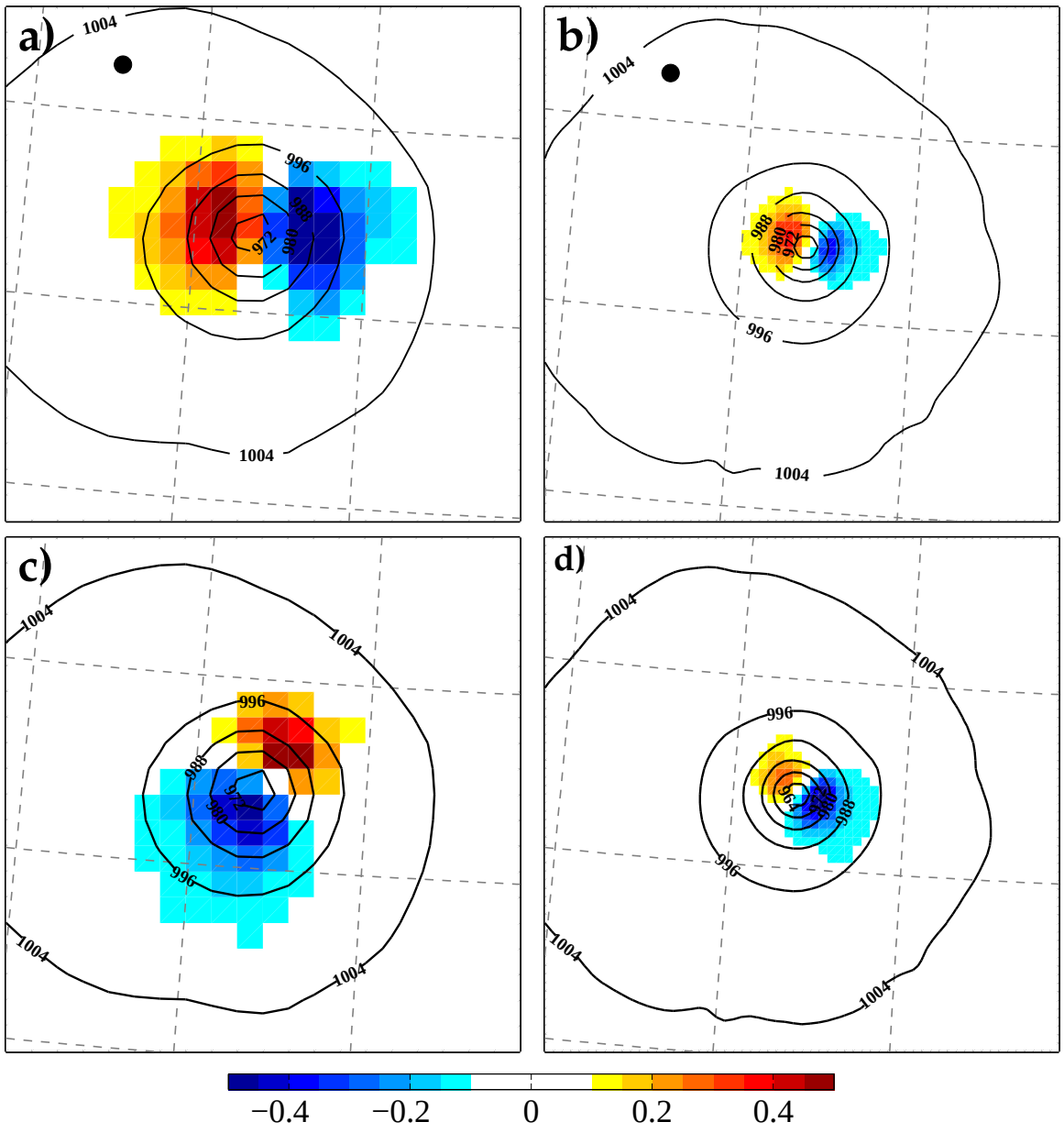

FIG. 2. Analysis increment of SLP (colors; hPa) on the (a) outer domain, and (b) inner domain obtained by assimilating one 500 hPa zonal wind dropsonde observation at the location indicated by the dot on 00 UTC 27 August 2005. The bottom row shows the leading analysis-increment EOF for the (c) outer domain and (d) inner domain. The EOFs are scaled to have maximum amplitude of 0.5. Contours are the ensemble-mean background SLP every 8 hPa. Latitude and longitude lines are shown every 2°.

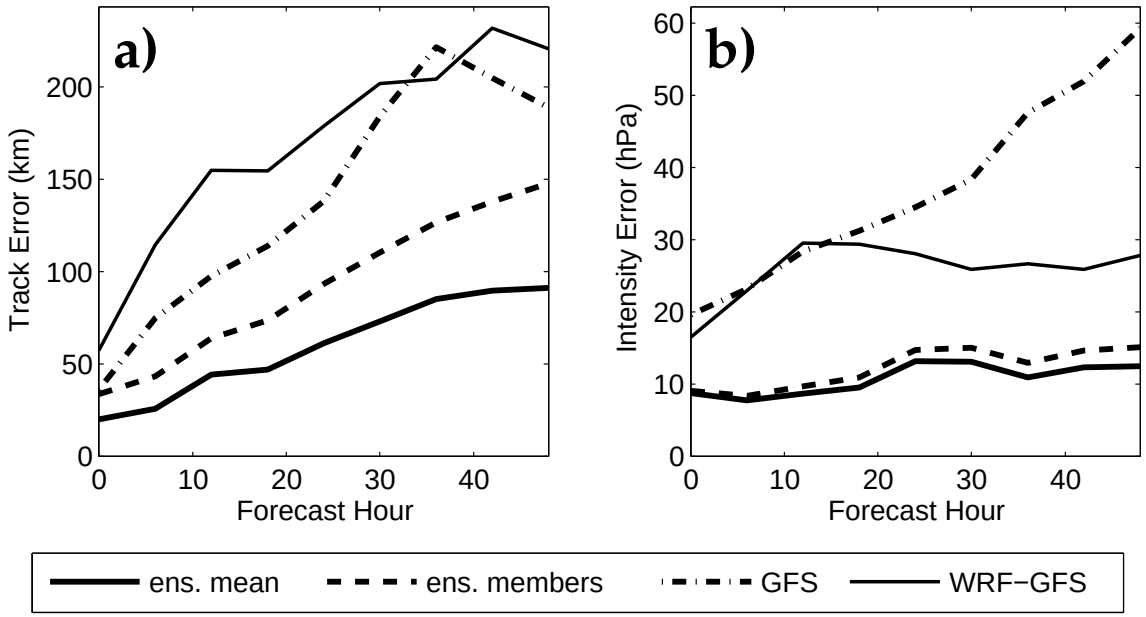

FIG. 3. RMS error in (a) tropical cyclone position and (b) tropical cyclone minimum central pressure as a function of forecast hour. The thick solid line is for the ensemble-mean forecast, the dashed line refers to the RMS error averaged over all ensemble members, the dot-dashed line is for GFS forecasts, and the thin solid line denotes the WRF forecast initialized from the GFS analysis. Forecasts apply to the outer domain and are initialized every 12 hours from 00 UTC 25 August 2005 to 00 UTC 27 August 2005.

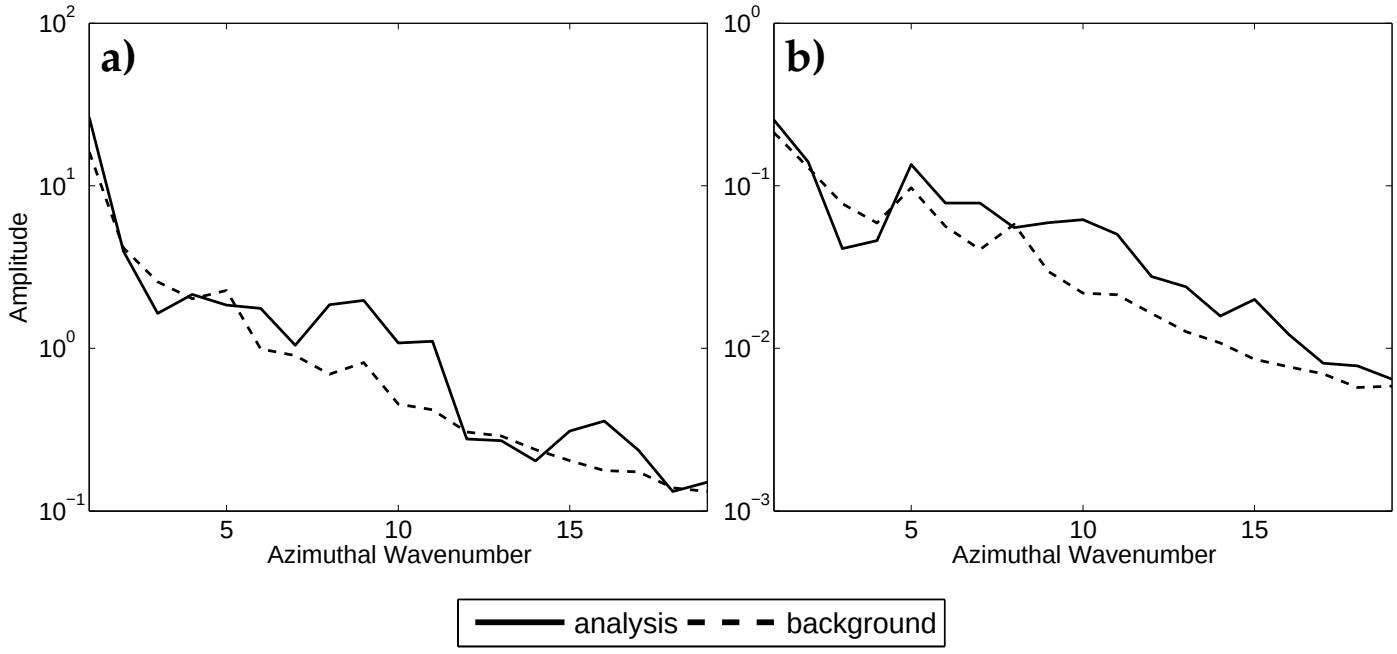

FIG. 4. Inner domain Fourier azimuthal amplitude spectrum of (a) sea-level pressure (hPa) and (b) 850 hPa temperature (K) for grid points within 100 km of the TC center before and after assimilating observations on 18 UTC 27 August 2005.

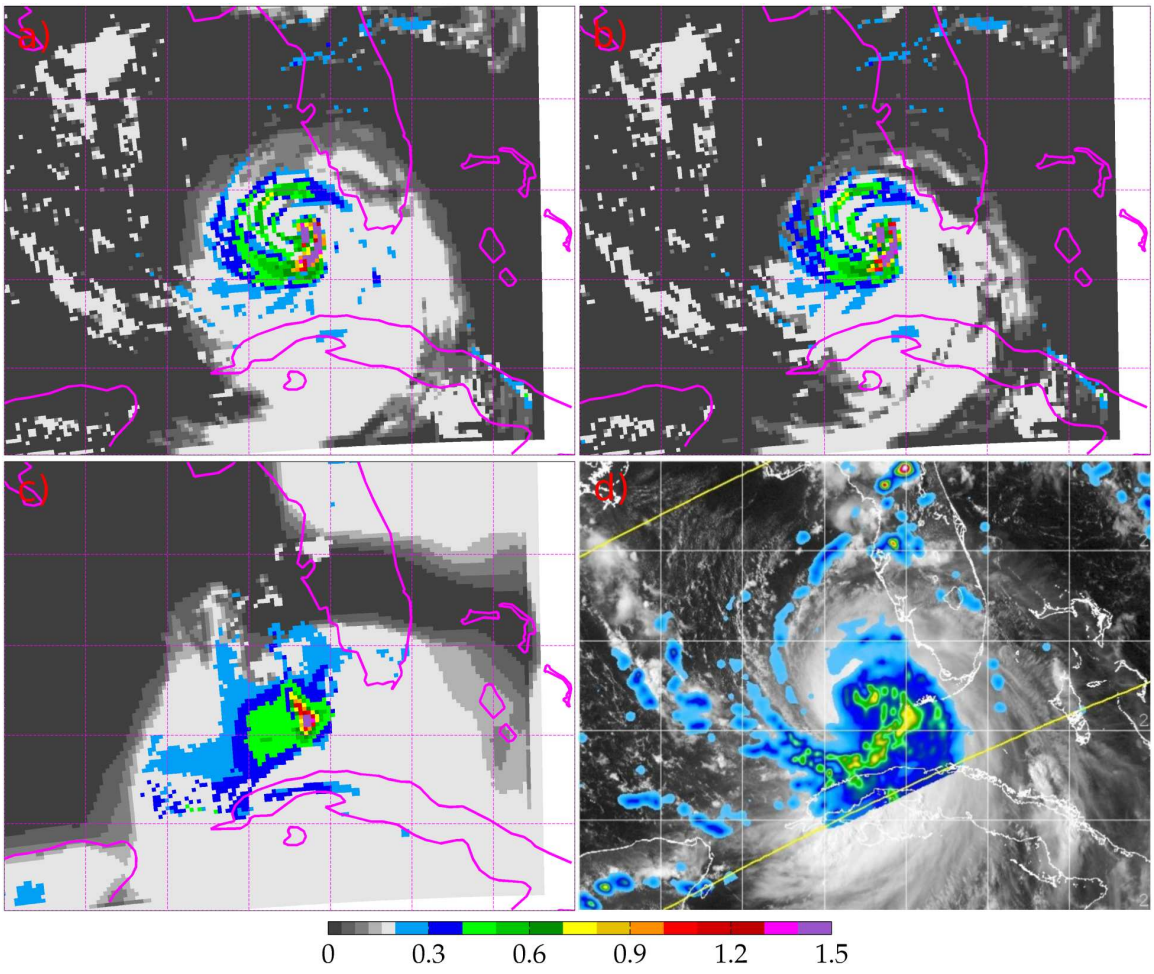

FIG. 5. (a) "full field", (b) "cold start", and (c) "GFS field" 45 minute forecasts of precipitation rate on the inner domain initialized on 21 UTC 26 August. Panel (d) shows the 2148 UTC TRMM satellite rain rate overlaid onto the 2045 UTC GOES-12 visible image (colors, inches hr^{-1}). White shading in panels (a)-(c) indicates the location of clouds in the model. The TRMM figure is courtesy of the Naval Research Laboratory Monterey Marine Meteorology Division.

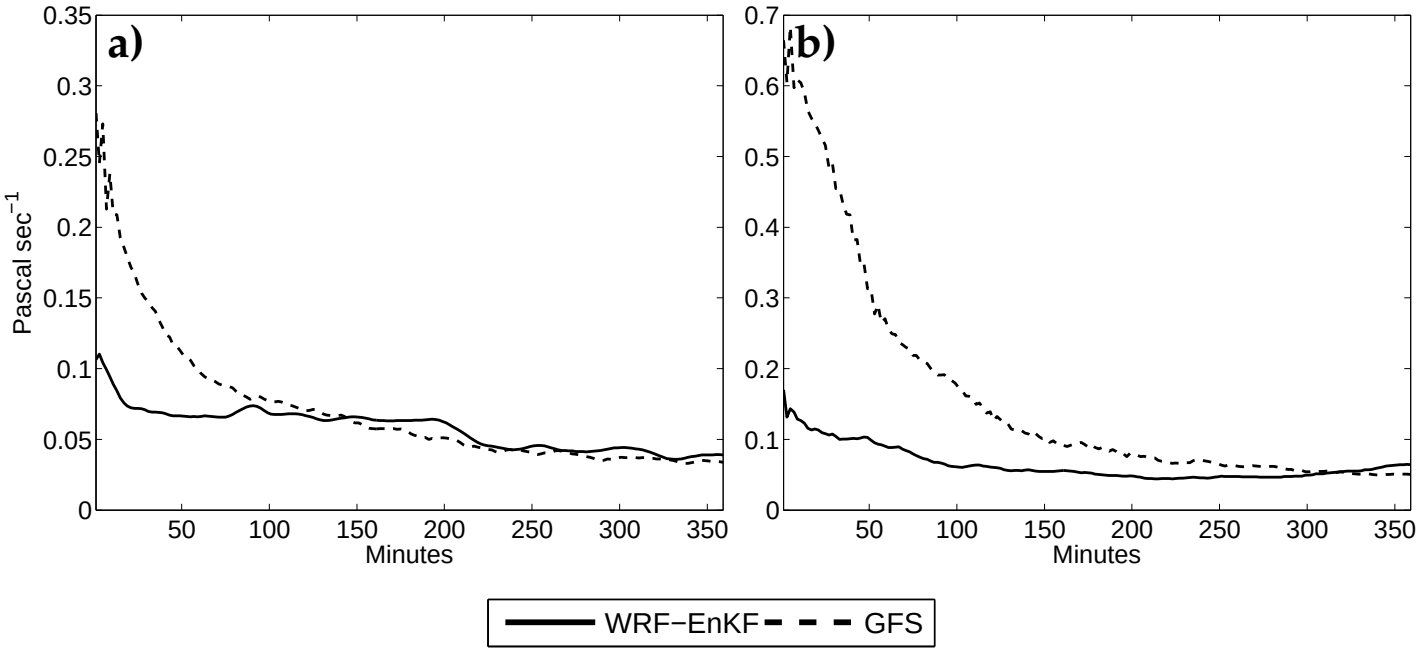

FIG. 6. RMS value of the derivative of WRF dry-air mass with respect to time within 600 km of the TC center as a function of lead time for an (a) outer and (b) inner domain forecast initialized from the 18 UTC 27 August 2005 WRF EnKF and GFS analysis.

List of Tables

TABLE 1. RMS Error in the ensemble-mean analysis (anal.) and background forecast (back.) of tropical cyclone track, minimum sea-level pressure and maximum 10 m wind.

	TC Track		TC min. SLP		TC max. wind	
Outer Domain						
	anal.	back.	anal.	back.	anal.	back.
Control	22 km	28 km	14.9 hPa	11.2 hPa	13.2 m s^{-1}	12.7 m s^{-1}
No Drop	22 km	28 km	14.6 hPa	11.3 hPa	13.5 m s^{-1}	12.4 m s^{-1}
No Best Track	31 km	46 km	24.3 hPa	20.1 hPa	16.8 m s^{-1}	17.0 m s^{-1}
Inner Domain						
	anal.	back.	anal.	back.	anal.	back.
Control	17 km	20 km	19.8 hPa	19.0 hPa	10.0 m s^{-1}	9.1 m s^{-1}
No Drop	18 km	22 km	47.8 hPa	43.5 hPa	13.5 m s^{-1}	13.0 m s^{-1}